analytical chemistry

pubs.acs.org/ac Article

Bioorthogonal Chemical Signature Enabling Amplified Visualization of Cellular Oxidative Thymines

Min Bai, Xiaowen Cao, Feng Chen, Jing Xue, Yue Zhao, and Yongxi Zhao*

Cite This: *Anal. Chem.* 2021, 93, 10495−10501 Read Online

ACCESS | Metrics & More | Article Recommendations | Supporting Information

ABSTRACT: Cellular oxidative thymines, 5-hydroxymethyluracil (5hmU) and 5-formyluracil (5fU), are found in the genomes of a diverse range of organisms, the distribution of which profoundly influence biological processes and living systems. However, the distribution of cellular oxidative thymines has not been explored because of lacking both specific bioorthogonal labeling and sensitivity methods for single-cell analysis. Herein, we report a bioorthogonal chemical signature enabling amplified visualization of cellular oxidative thymines in single cells. The synthesized ATP-γ-alkyne, an ATP analogue with bioorthogonal tag modified on γ-phosphate can be specifically linked to cellular 5hmU by chemoenzymatic labeling. DNA with 5-alkynephosphomethyluracil were then clicked with azide (N_3)-modified 5hmU-primer. Identification of 5fU is based on selective reduction from 5fU to 5hmU, subsequent chemoenzymatic labeling of the newly generated 5hmU, and cross-linking with N_3-modified 5fU-primer via click chemistry. Then, all of the 5hmU and 5fU sites are encoded with respective circularized barcodes. These barcodes are simultaneously amplified for multiplexed single-molecule imaging. The above two kinds of barcodes can be simultaneously amplified for differentiated visualization of 5hmU and 5fU in single cells. We find these two kinds of cellular oxidative thymines are spatially organized in a cell-type-dependent style with cell-to-cell heterogeneity. We also investigate their multilevel subcellular information and explore their dynamic changes during cell cycles. Further, using DNA sequencing instead of fluorescence imaging, our proposed bioorthogonal chemical signature holds great potential to offer the sequence information of these oxidative thymines in cells and may provide a reliable chemical biology approach for studying the whole-genome oxidative thymines profiles and insights into their functional role and dynamics in biology.

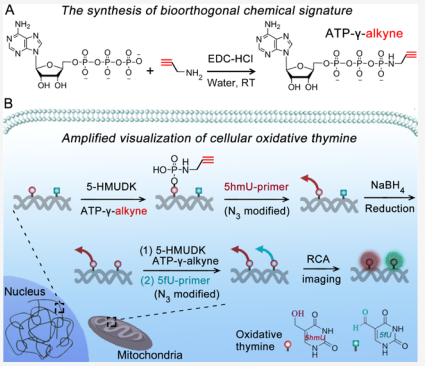

Numerous modified bases have been identified in the genomes of various organisms. They profoundly influence biological processes and living systems. These modified bases are implicated in pathological associations such as cancers,[1,2] among which the most widely studied ones are the derivatives of cytosine, including 5-methylcytosine (5mC) and its oxidized derivatives 5-hydroxymethylcytosine (5hmC), 5-formylcytosine (5fC), and 5-carboxycytosine (5caC).[3−7] However, the details of thymine modifications and their spatial distribution in cells remain elusive, especially cellular oxidative thymines. 5-Hydroxymethyluracil (5hmU) is an oxidation derivative of thymine determined in the genomes of sundry organisms.[8−10] In mammals, the levels of 5hmU are different in cells and tissue types.[11] Emerging evidence has demonstrated that 5hmU mononucleoside abundance can be used as a potential marker for the evaluation of breast cancer risk and invasiveness.[12,13] Recently, as the oxidation product of 5hmU or thymine, 5-formyluracil (5fU) was found in many cells and tissues.[8,14] 5fU can be generated by exposure to ultraviolet, reactive oxygen species, or ionizing radiation.[15−17] It is well known that 5fU is mutagenic and can induce transitional mutations. The inherent ability of strong electron-withdrawing 5-formyl group in 5fU contributes to gene miscoding and changes in DNA structures, which may cause DNA function disturbance.[18−20] Unfortunately, the abundance of 5hmU/5fU in the genome is very low, for example, ∼0.5−2.5 × 10^{-6} dN in mESCs.[8,21] The efficient analysis of low-abundance 5hmU/5fU in single cells is a major challenge. Especially, the structural similarity of 5fU and 5hmU hinders the differentiated detection of these two modifications. These factors make it extremely difficult to construct a sensitive and specific detection method for distinguishing between 5hmU and 5fU at the single-cell level.

So far, several methods have been developed for genomic 5hmU analysis by oxidation conversion of 5hmU to 5fU. Balasubramanian et al. employed polymerase extension to induce a change in the T to C bases due to the inherent ability of the resulting 5fU to form a pair of 5fU: G bases.[22] However, even under optimized conditions, the efficiency of this conversion is less than 40%. In addition, this method cannot

Received: March 24, 2021
Accepted: July 13, 2021
Published: July 22, 2021

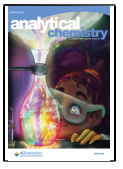

https://doi.org/10.1021/acs.analchem.1c01285
Anal. Chem. 2021, 93, 10495−10501

label intracellular 5hmU with bioorthogonal tags for in situ analysis. Another method biotinized 5fU with an aldehyder-eactive reagent.[23] However, this reagent also shows high reactivity to other aldehyde-containing modifications consisting in genomic DNA, especially 5fC. Therefore, this method can only achieve analysis of 5hmU with 5fU-, 5hmC-, and 5fC-absent DNA input. Recently, the enriching and sequencing of 5fU in mouse hippocampus was implemented by an azido derivative of (2-benzimidazolyl) acetonitrile.[24] Yet, simultaneous detection of cellular 5hmU and 5fU distribution has not been explored.

Cell imaging in situ can observe the subcellular distribution of biomolecules in single cells.[25−28] Antibody-labeled cellular immunofluorescence imaging has been used to detect high-abundance DNA modifications such as 5mC and 5hmC only in naked DNA.[29,30] Some base sites in condensed chromatins or masked by DNA-binding proteins may be sterically excluded from antibodies with relatively large sizes. Such noncovalent, affinity-based immunoassays have low binding efficiency and recognition specificity and are disabled to explore 5hmU and 5fU with low abundance. The rolling circle amplification (RCA) reaction is an isothermal signal amplification method. This method uses circular DNA as a template to convert DNA primer into long single-stranded DNA containing hundreds of repetitive sequences through enzymatic catalysis.[31−33] We previously reported a method to visualize single-cell 5-hydroxymethylpyrimidines based on the RCA reaction.[34] In this work, we have demonstrated that 5hmU DNA kinase (5-HMUDK) uses sulfhydryl-modified ATP-γ-S substrate to specifically phosphorylate 5hmU. Due to the large number of sulfhydryl proteins and molecules in cells, this method cannot be applied to the detection of 5hmU in dsDNA in the cellular environment. Therefore, constructing cellular-specific recognition of 5hmU/5fU with bioorthogonal tags and visualized analysis strategy in single cells is still challenging.

Herein, we developed a bioorthogonal chemical signature that enables amplified visualization of cellular 5hmU and 5fU (Scheme 1). First, we have synthesized an ATP analogue of γ-phosphate with biological orthogonal labeling, named ATP-γ-alkyne. After fixing the cells, ATP-γ-alkyne was used to label intracellular 5hmU by 5-HMUDK. Then, DNA with 5-alkynephosphomethyluracil (alkyne-5pmU) was further clicked with azide (N_3)-modified 5hmU-primer. Next, 5fU was reduced to 5hmU by water-soluble reductant, sodium borohydride ($NaBH_4$). The newly generated 5hmU sites were labeled with N_3-modified 5fU-primer by the phosphorylation and click reaction mentioned above. To simultaneously visualize the low abundance of 5hmU and 5fU in single cells, we performed RCA reaction and hybridization of fluorescent probes. Their spatial distributions in single cells and abundance differences in various cell types were further investigated. Furthermore, we explored their multilevel subcellular information and their dynamic changes during cell cycles.

Scheme 1. Schematic Diagrams for a Bioorthogonal Chemical Signature Enabling Amplified Visualization of Cellular Oxidative Thymines

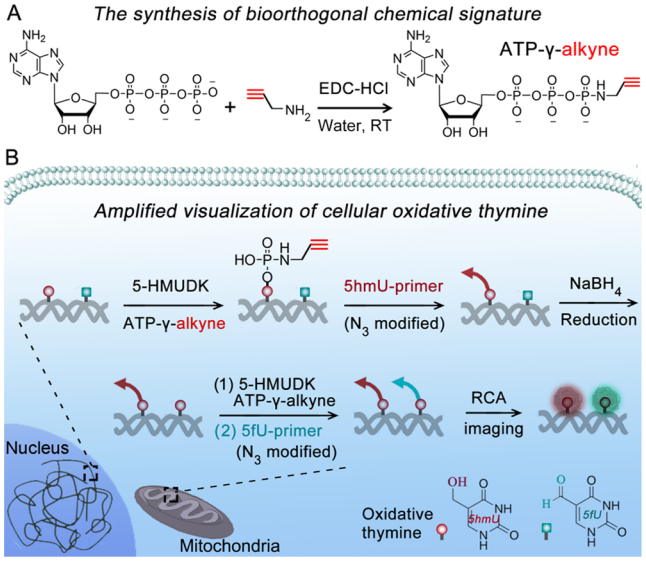

EXPERIMENTAL SECTION

Chemicals and Materials. Propargylamine, ATP disodium salt (adenosine 5′-triphosphate disodium salt), and 1-ethyl-3-(3-dimethyllamino-propyl)carbodiimide hydrochloride (EDC-HCl) were obtained from Sigma-Aldrich. Sodium ascorbate, sodium borohydride, and copper(II) sulfate were purchased from Aladdin. All of the reactions were performed in RNase-free water and buffers. Also, all chemical reagents were used as received without further purification. dfUTP and dhmUTP were obtained from Trilink Biotechnologies. The oligonucleotides of this work (Table S1) were prepared by Sangon Biological Co. Ltd. Exonuclease I, Exonuclease III, T4 DNA ligase, and DNase I were acquired from Takara Biotechnology Co. Ltd. 5-HMUDK, Klenow Fragment (3′ → 5′ exo-), hSMUG1, and phi29 DNA polymerase were acquired from New England Biolabs Ltd. Primary antibodies used in this study: H3K4me3, γH2AX, H3K4me1, and H3K27me3 were obtained from Cell Signaling Technology. MitoTracker Red CMTMRos and donkey antirabbit IgG (H+L) highly cross-adsorbed secondary antibody with Alexa fluor 488 were purchased from ThermoFisher Scientific. Antibody dilution buffers and blocking buffer were purchased from Beyotime Biotechnology.

Chemical Preparation of ATP-γ-Alkyne. ATP and propargylamine were used to prepare ATP-γ-alkyne. ATP disodium salt (4.9 mM) and propargylamine (245 mM) were dissolved in water.[35−37] The solution pH was adjusted to 6.0 with dilute HCl. Also, then EDC-HCl (490 mM) was added to the above solution and the mixture was stirred for 24 h at room temperature. Then, the pH of the solution was quickly adjusted to 8.5. After evaporating, silica column chromatography was used to purify the light yellow viscous products and obtain the powder product. ATP-γ-alkyne: high resolution mass spectrometry (HRMS) (ESI, negative mode) for $C_{13}H_{18}N_6O_{12}P_3$, $[M + H]^-$: 543.02010 (calculated), 543.01591 (found). All of the mass spectrometry analyses in this work were performed on a Waters I-Class Vion IMS Qtof with electrospray ionization. Nuclear magnetic resonance (NMR) spectra were recorded on a Brucker AVANCE III HD 600 MHz machine. The deuterated solvent in this work was D_2O. ^{31}P NMR spectra are referenced to H_3PO_4 as an external standard. Tetramethylsilane (TMS) was used as an external standard for ^{13}C NMR spectra.

5fU Reduced to 5hmU. Freshly prepared 3.5 μg/mL $NaBH_4$ solutions were slowly added to 10 μg/mL 5fU nucleobases solution. The mixture reaction was shaken at room temperature for 1 h in the dark. To stop the reaction,

https://doi.org/10.1021/acs.analchem.1c01285
Anal. Chem. 2021, 93, 10495−10501

750 mM sodium acetate (pH 5) was added the mixture until no gas was released. The efficiency of 5fU reduction was characterized by UV−vis absorption spectra.

Reactions of 5hmU Phosphorylation by 5-HMUDK. The double-stranded DNA substrates containing a single 5hmU:A site were synthesized by polymerization extension of a primer-template duplex. To verify the feasibility of 5hmU phosphorylation by 5-HMUDK, 4 μL of double-stranded DNA substrate (50 μM), 1 μL of 5-HMUDK (20 U/μL), and 1 μL of ATP-γ-alkyne (10 mM) was incubated in 20 μL of 1× Cutsmart buffer for 1 h at 37 °C. *Nco*I-HF (0.5 μL; 20 U/μL) was used to cut the phosphorylation products in 20 μL of 1× Cutsmart buffer for 1 h at 37 °C. The efficiency of 5hmU phosphorylation was characterized by melting curve analysis.

Synthesis of Circularized Padlocks. Hybridization, ligation, and digestion are the main reaction processes in the preparation of circularized padlocks. First, the hybridization was operated in T4 DNA ligase reaction buffer (10 μL), which contained 2 μL of padlock probes (50 μM) and 3 μL of ligation linker (100 μM) for 2 h at 55 °C. Second, added 700 U T4 DNA ligase to catalyze the ligation of 3′ hydroxyl and 5′ phosphate termini of padlock probes. After reacting for 2 h at 37 °C, the mixture was inactivated at 65 °C for 40 min. Finally, excess exonuclease was added to digest all of the linear DNA overnight at 37 °C. Next, 80 °C for 40 min to inactivate all of the enzymes.

Visualizing Intracellular 5hmU and 5fU. Breast cell lines MCF-10A, MCF-7, and MDA-MB-231 cells were cultured in DEME with 1% antibiotic penicillin−streptomycin (100 U/mL) and 10% FBS at 37 °C.

Then, 6000 cells were inoculated overnight on collagen-A-coated cover glass in the poly(dimethylsiloxane) (PDMS) chamber at 37 °C. Then, the cells were fixed with 4% formaldehyde at room temperature for 10 min. To permeate the cells, the cells were cultured with 0.5% Triton X-100 in phosphate-buffered saline (PBS) for 5 min. After washing the cells three times with PBST, we first labeled it as intercellular 5hmU. For a typical 5hmU phosphorylation reaction, the cells were incubated with 1 μL of 5-HMUDK (20 U/μL) and 500 μM ATP-γ-alkyne in 1× Cutsmart buffer at 37 °C for 2 h. Then, the mixed solution containing 250 nM 5hmU barcode probe, 1 mM copper(II) sulfate, 100 mM sodium ascorbate, and 0.5 μg/mL sperm DNA was added to perform a copper(I)-catalyzed click reaction at room temperature for 1 h in dark. Excess probes and molecules were carefully washed three times. Next, 5fU was reduced to 5hmU with 1 mg/mL $NaBH_4$ for 5 min at room temperature in dark. After washing several times until no bubbles, the newly generated 5hmU was labeled with a 5fU barcode probe by the phosphorylation and click reaction mentioned above.

For the RCA reaction, two circularized padlocks (200 nM each), 0.5 μg/mL sperm DNA, 20% formamide, and 2× SSC formed a ring template hybrid reaction system. Then, the hybridization mixture was reacted with the fixed cells at 37 °C for 3 h. Next, barcoding of RCA reaction was performed in 10 μL of 1× phi29 DNA polymerase buffer containing 0.5 μL of phi29 DNA polymerase (10 U/μL), 0.5 μL of BSA (10 mg/mL), and 2.5 mM dNTPs at 37 °C for 2 h. After the cells were washed three times, fluorophore-labeled DNA probes (200 nM each) in 2× SSC buffer with 20% formamide were incubated with the samples at 37 °C for 30 min. 4′,6-Diamidino-2-phenylindole (DAPI) is used to stain the nucleus. In this work, MitoTracker Red CMTMRos was used to stain the mitochondria at 37 °C for 20 min before cell fixation. The G1, S, and G2 phases of cells were synchronized with lovastatin, hydroxylurea, and colchicine, respectively. For immunostaining of histone, the cells were first blocked for 1 h in QuickBlock blocking buffer at room temperature. Then, the cells were incubated with primary antibody H3K4me1 (1:800), H3K4me3 (1:400), H3K27me3 (1:1600), and γH2AX (1:400) diluted by QuickBlock primary antibody dilution buffer overnight at 4 °C. After washing, the fluorescent secondary antibody was added to image the histones at room temperature for 1 h.

All fluorescence images were acquired using laser scanning confocal microscopy (TCS SP8 STED 3X, Leica). The cell images in this work were captured using a 63× water objective (NA 1.2). We randomly selected the cells to analyze. We used Matlab 2019b to extract the spot count and fluorescence intensity of single cells.

RESULTS AND DISCUSSION

First, ATP-γ-alkyne was synthesized by a coupling reaction of ATP with propargylamine using EDC-HCl as the activator in water at pH 6.0. The purified reaction mixtures were analyzed by mass spectrometry (MS). As shown in Figure 1A, the MS spectrum peak of ATP-γ-alkyne in the negative-ion mode was 543.01591, which was consistent with its theoretical molecular

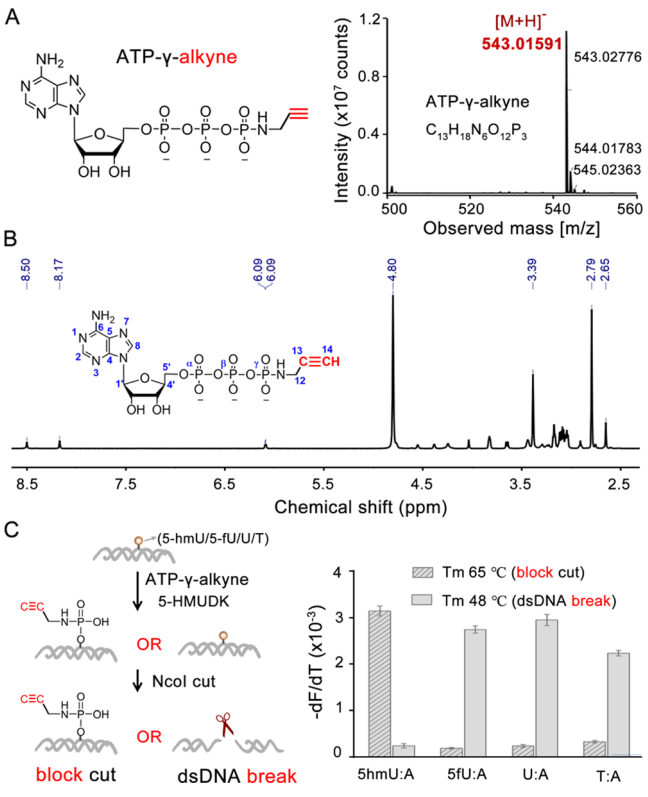

Figure 1. Synthesis and characterization of ATP-γ-alkyne. (A) Chemical structure and mass spectrum of ATP-γ-alkyne ($C_{13}H_{18}N_6O_{12}P_3$, $[M + H]^-$, calculated: 543.02010, found: 543.01591). (B) ^{1}H NMR spectrum of ATP-γ-alkyne. ^{1}H NMR (600 MHz,D_2O): δ (ppm) = 8.50 (s, 1H, 2H), 8.17 (s, 1H, H8), 6.09 (d, J = 6.09 Hz, 1H, H1′), 4.80 (m, 1H, overlapping with HOD, H2′), 4.61−4.54 (m, 1H, H3′), 4.38 (m, 1H, H4′), 4.24 (m, 2H, H5′), 2.79−2.65 (m, 3H, H12, H14). (C) Melting temperature of model dsDNA samples cut by restricting endonuclease *Nco*I-HF.

https://doi.org/10.1021/acs.analchem.1c01285
Anal. Chem. 2021, 93, 10495−10501

weight. The coupling reaction with complete selectivity at the γ-phosphate has been proved by ^{1}H, ^{13}C, and ^{31}P NMR spectroscopy (Figures 1B, S1, and S2).

Next, we studied whether 5-HMUDK used our synthesized bioorthogonal ATP analogue to alkynephosphorylate 5hmU site in double-stranded DNA. This double-stranded DNA containing different modification sites and restriction endonuclease *Nco*I-HF recognition sequences was prepared as 5-HMUDK substrates. DNA melting temperatures were used to detect double-stranded DNA breaks; all of the double-stranded DNA substrates were treated with ATP-γ-alkyne. As shown in Figure 1C, only the 5hmU:A sample blocked DNA break after the *Nco*I-HF excision reaction. This is because the phosphorylation of 5hmU protects it from being cleaved by *Nco*I-HF restriction endonuclease. Thus, ATP-γ-alkyne was proven to be an efficient alkynephosphate donor for 5-HMUDK to specifically mark 5hmU.

To visualize intracellular 5hmU and obtain the spatial distribution information in single cells, we next developed a bioorthogonal chemical-signature-encoded DNA amplification strategy. Specifically, the resulting ATP-γ-alkyne with bioorthogonal tag was used to label intracellular 5hmU. To introduce DNA amplification, 5′ azide (N_3)-modified DNA primer (5hmU-primer) reacted with the generated alkyne-5pmU. This primer could trigger RCA reaction and produce a tandem periodic long single DNA strand, which can capture many molecules of fluorescence probes for signal amplification. As shown in Figure 2A, the spot number was used to roughly assess the number of 5hmU sites in the cells. Greater spot count and fluorescence signal were observed in these RCA-treated single cells compared to no RCA, which made it possible to visualize low-abundance modified bases. Notably, intracellular 5hmU count is single-cell heterogeneous. To verify the specificity of our method, we performed a series of negative experiments. In detail, we processed hSMUG1 prior to the alkynphosphorylation reaction to prepare the 5hmU defective sample. The other negative experiment had no 5-HMUDK. From the cell imaging results, negligible adsorption background fluorescence or nonspecific labeling was observed in a series of negative samples. These results proved the cellular genomic 5hmU-specific amplified visualization in single-cell samples by our method. As shown in Figure 2B, primer-probe was subsequently added. No RCA fluorescence signal of 5fU-primer-probe was observed. This indicated that all 5hmU modification sites were cross-linked with 5hmU-primer after the click reaction, and there were no residual sites to interfere with subsequent 5fU labeling. Further, the reduction of 5fU to 5hmU was investigated. In the previous work, the water-soluble reducing agent $NaBH_4$ was used to reduce 5fC in genomic DNA to 5hmC.[38] $NaBH_4$ also can reduce 5fU to 5hmU (Figure 2C). From the above results, we can detect 5fU by 5hmU labeling method catalyzed by 5-HMUDK after $NaBH_4$ reduction. These results may enable the joint analysis of 5fU and 5hmU in the same single cells following a proper order.

Next, we would visualize intracellular 5hmU and 5fU via the bioorthogonal chemical-signature-encoded DNA amplification method. Specifically, ATP-γ-alkyne was first used to label intracellular 5hmU in single cells. The resulting alkyne-5pmU in DNA were further clicked with 5hmU-primer. Next, intracellular 5fU was reduced to 5hmU by $NaBH_4$. The newly generated 5hmU was labeled with 5fU barcode primer (5fU-primer) by the phosphorylation and click reaction

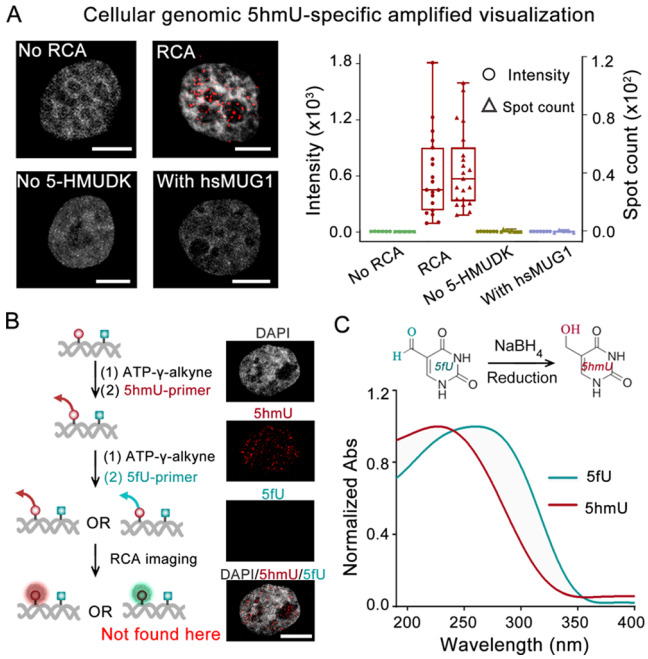

Figure 2. Bioorthogonal labeling and imaging of 5hmU in cells. (A) Cellular genomic 5hmU-specific amplified visualization using 5-HMUDK and ATP-γ-alkyne. Left: representative cell images (merged picture: red, 5hmU; gray, DAPI) of single cells with different conditions. Right: the corresponding spot count and fluorescence intensity analysis. The cell numbers are 50. (B) Results of all intracellular 5hmU sites were cross-linked with DNA probes (red spot), and no residual sites were detected (green spot). (C) Absorption spectra for 5fU reduction characterization. Green line: absorption spectrum of 5fU; red line: absorption spectrum of reduction product 5hmU. MCF-10A cells were used. Scale bars of cell images are 10 μm in this work.

mentioned above. To simultaneously visualize the low abundance of 5hmU and 5fU in single cells, we performed RCA reaction and hybridization of fluorescent probes. Figure 3B shows representative merged images for the spatial distributions of 5hmU and 5fU in different human breast cell lines, including nontumorigenic MCF-10A and carcinogenic MCF-7 and MDA-MB-231. In addition, the spot count and fluorescence intensity of individual cells in different cell lines were statistically analyzed (Figures 3C, S3, and S4). The results showed that, despite significant single-cell heterogeneity, the mean spots/cells and fluorescence intensity/cells of 5hmU and 5fU in MCF-7 were significantly higher than those of MCF-10A and MDA-MB-231. Subsequently, we investigated the colocalization of 5hmU and 5fU. The violin chart shows Pearson's correlation coefficient between the 5hmU signal and the 5fU signal of each cell in different cell types (Figure 3D). The high colocalization values for these two modifications in different cancer cell lines may imply their potential correlation in the cells. Especially, 5fU may be derived from 5hmU in mammalians. Overall, all these observations revealed that the spatial distributions and the correlation of 5hmU and 5fU in DNA differed between three breast cell lines.

Then, we profiled the changes of 5hmU and 5fU during cell cycles. MDA-MB-231 cells were synchronized in G1, S, and G2 phases, respectively. Figure 4A shows the representative merged images of the cells. We performed a statistical analysis of 5hmU and 5fU spot counts and signal intensities in single

https://doi.org/10.1021/acs.analchem.1c01285
Anal. Chem. 2021, 93, 10495−10501

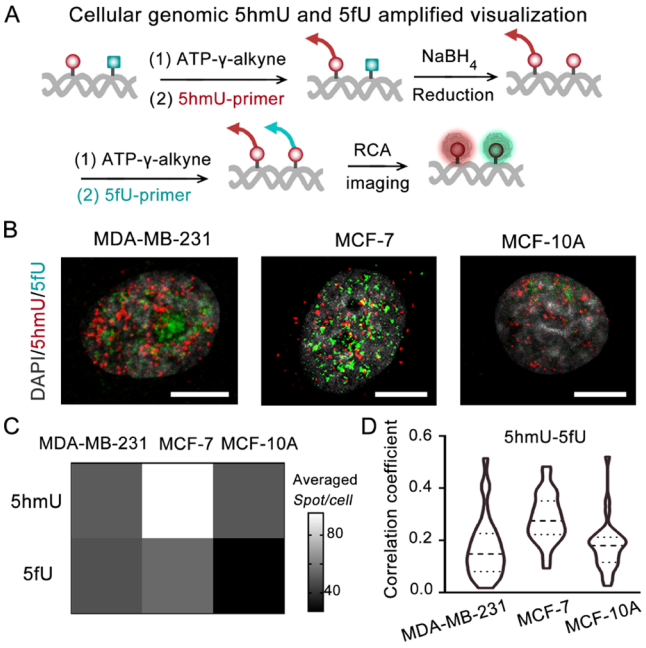

Figure 3. Conjoint analysis of 5hmU and 5fU in three breast cell lines. (A) Mechanism of cellular genomic 5hmU- and 5fU-amplified visualization. (B) Representative merged cell images of three breast cell lines (merged: gray, DAPI; red, 5hmU; green, 5fU). (C) Statistical analysis of changes in mean 5hmU and 5fU spot counts of a single cell in three breast cell lines. The cell numbers are 50. (D) Pearson's correlation coefficients between 5hmU signal and 5fU signal in different cell types.

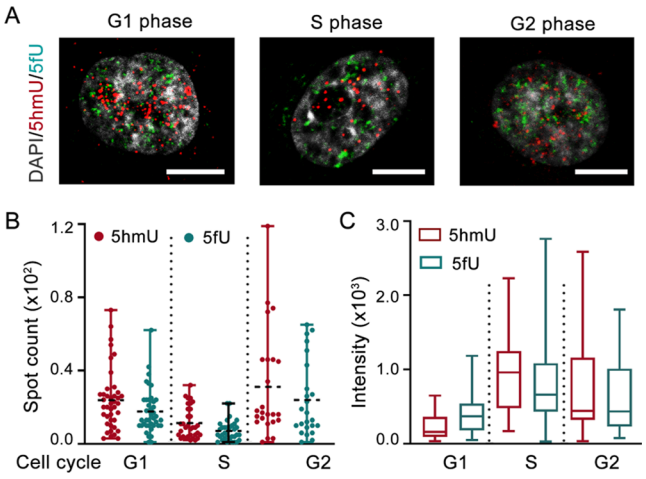

Figure 4. Exploring changes of single-cell 5hmU and 5fU during cell cycles. (A) Representative single-cell images for G1, S, and G2 phases of the cell cycle (merged: gray, DAPI; red, 5hmU; green, 5fU). (B) Statistical analysis of spot count for single-cell 5hmU and 5fU during cell cycles. The cell numbers are 50. (C) Statistical analysis of fluorescence intensity for single-cell 5hmU and 5fU during cell cycles. The cell numbers are 50. MDA-MB-231 cells were used here.

cells during cell cycles (Figure 4B,C). Judging from the spot counts, as the cell cycle changes, 5hmU and 5fU do not show a significant pattern. However, it could be seen from the signal intensities that the intensities of 5hmU and 5fU in the G1 phase were lower than those in the S and G2 phases. This may be related to the process of DNA or chromatin replication.

As we all know, in addition to DNA in the nucleus, mitochondria also contain DNA. To verify whether there are chemical modifications on the DNA in mitochondria, we performed a colocalization analysis between 5hmU/5fU signal and MitoTracker signal. The representative cell images of different cell lines (MCF-10A, MCF-7, MDA-MB-231) are shown in Figure 5A. The violin plot represents the correlation

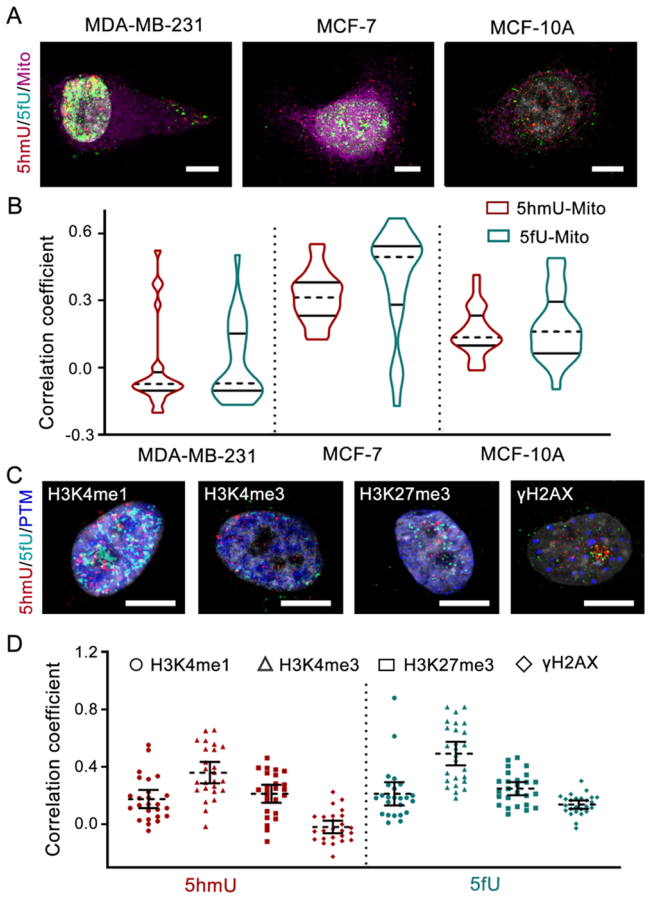

Figure 5. Multilevel subcellular distribution analysis of 5hmU and 5fU. (A) Representative cell images of 5hmU and 5fU labeling with MitoTracker imaging to study mitochondrial oxidative thymines (merged: gray, DAPI; red, 5hmU; green, 5fU; purple: mitochondria, abbreviation as Mito). (B) Pearson's correlation coefficients between 5hmU/5fU signal and MitoTracker signal in different cell types. The cell numbers are 50. (C) Representative cell images of 5hmU and 5fU labeling with four histone modifications imaging (merged: gray, DAPI; red, 5hmU; green, 5fU; blue: histone modification). (D) Pearson's correlation coefficients between 5hmU/5fU signal and histone modifications. The cell numbers are 50.

coefficients between 5hmU/5fU signal and MitoTracker signal in different cell types. As shown in Figure 5B, the correlation coefficient between 5hmU/5fU and mitochondria in carcinogenic MCF-7 is higher than that of MCF-10A and MDA-MB-231, especially 5fU. Thus, we also investigated the spatial relationship between two oxidative thymines and histone modifications such as H3K4me1, H3K4me3, H3K27me3, or γH2AX. The representative cell images are shown in Figure 5C. We observed high fluorescence colocalization rates for 5hmU/H3K4me1, 5hmU/H3K4me3, 5hmU/H3K27me3, 5fU/H3K4me1, 5fU/H3K4me3, and 5fU/H3K27me3 despite remarkable single-cell heterogeneity (Figure 5D). These results indicate the potential relationship between these three histone modifications and DNA methylation.

https://doi.org/10.1021/acs.analchem.1c01285
Anal. Chem. 2021, 93, 10495−10501

CONCLUSIONS

In summary, we developed a bioorthogonal chemical-signature-encoded DNA amplification method for visualization of cellular oxidative thymines. To accomplish this, we have synthesized a new ATP analogue with a bioorthogonal tag modified on γ-phosphate, ATP-γ-alkyne. It was able to use as an efficient alkynephosphate donor for 5-HMUDK to specifically mark cellular 5hmU. Combined with $NaBH_4$ reduction and RCA, conjoint analysis of 5hmU and 5fU in the same single cells was realized following a proper labeling order. Next, we revealed the cell-type-specific characteristics of 5hmU and 5fU with single-cell variants. We also found their differences in multilevel subcellular information and dynamic changes during cell cycles. The combination of this bioorthogonal chemoenzymatic method can quantify and precisely map these two oxidative thymines in the genome and help providing insights into their function.

ASSOCIATED CONTENT

Supporting Information

The Supporting Information is available free of charge at https://pubs.acs.org/doi/10.1021/acs.analchem.1c01285.

Table S1: sequence information for oligonucleotides used in this work; Figure S1: ^{13}C NMR spectra of ATP-γ-alkyne; Figure S2: ^{31}P NMR spectra of ATP-γ-alkyne; Figure S3: statistical analysis of single-cell spot count of 5hmU and 5fU in different cell lines; Figure S4: statistical analysis of single-cell fluorescence intensity of 5hmU and 5fU in different cell lines; and supplementary figures and data (PDF)

AUTHOR INFORMATION

Corresponding Author

Yongxi Zhao − *Institute of Analytical Chemistry and Instrument for Life Science, The Key Laboratory of Biomedical Information Engineering of Ministry of Education, School of Life Science and Technology, Xi'an Jiaotong University, Xi'an 710049 Shaanxi, P. R. China;* orcid.org/0000-0002-1796-7651; Email: yxzhao@mail.xjtu.edu.cn

Authors

Min Bai − *Institute of Analytical Chemistry and Instrument for Life Science, The Key Laboratory of Biomedical Information Engineering of Ministry of Education, School of Life Science and Technology, Xi'an Jiaotong University, Xi'an 710049 Shaanxi, P. R. China*

Xiaowen Cao − *Institute of Analytical Chemistry and Instrument for Life Science, The Key Laboratory of Biomedical Information Engineering of Ministry of Education, School of Life Science and Technology, Xi'an Jiaotong University, Xi'an 710049 Shaanxi, P. R. China*

Feng Chen − *Institute of Analytical Chemistry and Instrument for Life Science, The Key Laboratory of Biomedical Information Engineering of Ministry of Education, School of Life Science and Technology, Xi'an Jiaotong University, Xi'an 710049 Shaanxi, P. R. China;* orcid.org/0000-0003-0188-6256

Jing Xue − *Institute of Analytical Chemistry and Instrument for Life Science, The Key Laboratory of Biomedical Information Engineering of Ministry of Education, School of Life Science and Technology, Xi'an Jiaotong University, Xi'an 710049 Shaanxi, P. R. China*

Yue Zhao − *Institute of Analytical Chemistry and Instrument for Life Science, The Key Laboratory of Biomedical Information Engineering of Ministry of Education, School of Life Science and Technology, Xi'an Jiaotong University, Xi'an 710049 Shaanxi, P. R. China*

Complete contact information is available at: https://pubs.acs.org/10.1021/acs.analchem.1c01285

Author Contributions

All authors have given approval to the final version of the manuscript.

Notes

The authors declare no competing financial interest.

ACKNOWLEDGMENTS

This research was supported by the China Postdoctoral Science Foundation (Grant Numbers 2020M683448 and 2019M663658), the National Natural Science Foundation of China (Grant Numbers 92068118 and 21874105), the Natural Science Basic Research Program of Shaanxi (Grant Number 2020JQ-021), the Fundamental Research Funds for the Central Universities, and "Young Talent Support Plan" of Xi'an Jiaotong University. The authors thank Hao at the Instrument Analysis Center of Xi'an Jiaotong University for her assistance with fluorescence imaging analysis.

REFERENCES

(1) Berney, M.; McGouran, J. F. *Nat. Rev. Chem.* **2018**, *2*, 332−348.

(2) Zhao, L. Y.; Song, J. H.; Liu, Y. B.; Song, C. X.; Yi, C. Q. *Protein Cell* **2020**, *11*, 792−808.

(3) Bachman, M.; Uribe-Lewis, S.; Yang, X. P.; Williams, M.; Murrell, A.; Balasubramanian, S. *Nat. Chem.* **2014**, *6*, 1049−1055.

(4) Liu, C.; Cui, X. L.; Zhao, B. X.; Narkhede, P.; Gao, Y. W.; Liu, J.; Dou, X. Y.; Dai, Q.; Zhang, L. S.; He, C. *J. Am. Chem. Soc.* **2020**, *142*, 4539−4543.

(5) Liu, Y. B.; Siejka-Zielinska, P.; Velikova, G.; Bi, Y.; Yuan, F.; Tomkova, M.; Bai, C. S.; Chen, L.; Schuster-Bockler, B.; Song, C. X. *Nat. Biotechnol.* **2019**, *37*, 424−429.

(6) Schutsky, E. K.; DeNizio, J. E.; Hu, P.; Liu, M. Y.; Nabel, C. S.; Fabyanic, E. B.; Hwang, Y.; Bushman, F. D.; Wu, H.; Kohli, R. M. *Nat. Biotechnol.* **2018**, *36*, 1083−1090.

(7) Xia, B.; Han, D. L.; Lu, X. Y.; Sun, Z. Z.; Zhou, A. K.; Yin, Q. Z.; Zeng, H.; Liu, M. H.; Jiang, X.; Xie, W.; He, C.; Yi, C. Q. *Nat. Methods* **2015**, *12*, 1047−1050.

(8) Pfaffeneder, T.; Spada, F.; Wagner, M.; Brandmayr, C.; Laube, S. K.; Eisen, D.; Truss, M.; Steinbacher, J.; Hackner, B.; Kotljarova, O.; Schuermann, D.; Michalakis, S.; Kosmatchev, O.; Schiesser, S.; Steigenberger, B.; Raddaoui, N.; Kashiwazaki, G.; Muller, U.; Spruijt, C. G.; Vermeulen, M.; Leonhardt, H.; Schar, P.; Muller, M.; Carell, T. *Nat. Chem. Biol.* **2014**, *10*, 574−581.

(9) Modrzejewska, M.; Gawronski, M.; Skonieczna, M.; Zarakowska, E.; Starczak, M.; Foksinski, M.; Rzeszowska-Wolny, J.; Gackowski, D.; Olinski, R. *Free Radical Biol. Med.* **2016**, *101*, 378−383.

(10) Olinski, R.; Starczak, M.; Gackowski, D. *Mutat. Res.* **2016**, *767*, 59−66.

(11) Liu, S.; Wang, J.; Su, Y. J.; Guerrero, C.; Zeng, Y. X.; Mitra, D.; Brooks, P. J.; Fisher, D. E.; Song, H. J.; Wang, Y. S. *Nucleic Acids Res.* **2013**, *41*, 6421−6429.

(12) Djuric, Z.; Heilbrun, L. K.; Lababidi, S.; Berzinkas, E.; Simon, M. S.; Kosir, M. A. *Cancer Epidemiol. Biomarkers Prev.* **2001**, *10*, 147−149.

(13) Frenkel, K.; Karkoszka, J.; Glassman, T.; Dubin, N.; Toniolo, P.; Taioli, E.; Mooney, L. A.; Kato, I. *Cancer Epidemiol. Biomarkers Prev.* **1998**, *7*, 49−57.
(14) Hong, H. H.; Wang, Y. S. *Anal. Chem.* **2007**, *79*, 322−326.
(15) Decarroz, C.; Wagner, J. R.; Vanlier, J. E.; Krishna, C. M.; Riesz, P.; Cadet, J. *Int. J. Radiat. Biol. Relat. Stud. Phys., Chem. Med.* **1986**, *50*, 491−505.
(16) Hong, H. Z.; Cao, H. C.; Wang, Y. S.; Wang, Y. S. *Chem. Res. Toxicol.* **2006**, *19*, 614−621.
(17) Kasai, H.; Iida, A.; Yamaizumi, Z.; Nishimura, S.; Tanooka, H. *Mutat. Res. Lett.* **1990**, *243*, 249−253.
(18) Kawasaki, F.; Murat, P.; Li, Z.; Santner, T.; Balasubramanian, S. *Chem. Commun.* **2017**, *53*, 1389−1392.
(19) Rogstad, D. K.; Heo, J.; Vaidehi, N.; Goddard, W. A.; Burdzy, A.; Sowers, L. C. *Biochemistry* **2004**, *43*, 5688−5697.
(20) Yoshida, M.; Makino, K.; Morita, H.; Terato, H.; Ohyama, Y.; Ide, H. *Nucleic Acids Res.* **1997**, *25*, 1570−1577.
(21) Hofer, A.; Liu, Z. J.; Balasubramanian, S. *J. Am. Chem. Soc.* **2019**, *141*, 6420−6429.
(22) Kawasaki, F.; Cuesta, S. M.; Beraldi, D.; Mahtey, A.; Hardisty, R. E.; Carrington, M.; Balasubramanian, S. *Angew. Chem., Int. Ed.* **2018**, *57*, 9694−9696.
(23) Kawasaki, F.; Beraldi, D.; Hardisty, R. E.; McInroy, G. R.; van Delft, P.; Balasubramanian, S. *Genome Biol.* **2017**, *18*, No. 23.
(24) Wang, Y. F.; Liu, C. X.; Wu, F.; Zhang, X.; Liu, S.; Chen, Z. G.; Zeng, W. W.; Yang, W.; Zhang, X. L.; Zhou, Y.; Weng, X. C.; Wu, Z. G.; Zhou, X. *iScience* **2018**, *9*, 423−432.
(25) Xue, J.; Chen, F.; Su, L.; Cao, X. W.; Bai, M.; Zhao, Y.; Fan, C. H.; Zhao, Y. X. *Angew. Chem.* **2021**, *133*, 3470−3474.
(26) Ren, X. J.; Zhang, K. X.; Deng, R. J.; Li, J. H. *Chem* **2019**, *5*, 2571−2592.
(27) Li, S. Q.; Liu, Y. R.; Liu, L.; Feng, Y. M.; Ding, L.; Ju, H. X. *Angew. Chem., Int. Ed.* **2018**, *57*, 12007−12011.
(28) Zhang, Z.; Wang, Y. Y.; Zhang, N. B.; Zhang, S. S. *Chem. Sci.* **2016**, *7*, 4184−4189.
(29) Zhong, S. W.; Li, Z.; Jiang, T.; Li, X. J.; Wang, H. L. *Anal. Chem.* **2017**, *89*, 5702−5707.
(30) Ficz, G.; Branco, M. R.; Seisenberger, S.; Santos, F.; Krueger, F.; Hore, T. A.; Marques, C. J.; Andrews, S.; Reik, W. *Nature* **2011**, *473*, 398−U589.
(31) Ge, J.; Zhang, L. L.; Liu, S. J.; Yu, R. Q.; Chu, X. *Anal. Chem.* **2014**, *86*, 1808−1815.
(32) Zhu, G. Z.; Hu, R.; Zhao, Z. L.; Chen, Z.; Zhang, X. B.; Tan, W. H. *J. Am. Chem. Soc.* **2013**, *135*, 16438−16445.
(33) Larsson, C.; Koch, J.; Nygren, A.; Janssen, G.; Raap, A. K.; Landegren, U.; Nilsson, M. *Nat. Methods* **2004**, *1*, 227−232.
(34) Chen, F.; Xue, J.; Zhang, J.; Bai, M.; Yu, X.; Fan, C. H.; Zhao, Y. X. *J. Am. Chem. Soc.* **2020**, *142*, 2889−2896.
(35) Chen, F.; Bai, M.; Cao, X. W.; Xue, J.; Zhao, Y.; Wu, N.; Wang, L.; Zhang, D. X.; Zhao, Y. X. *Nat. Commun.* **2021**, *12*, No. 1965.
(36) Hacker, S. M.; Mex, M.; Marx, A. *J. Org. Chem.* **2012**, *77*, 10450−10454.
(37) Serdjukow, S.; Kink, F.; Steigenberger, B.; Tomas-Gamasa, M.; Carell, T. *Chem. Commun.* **2014**, *50*, 1861−1863.
(38) Booth, M. J.; Marsico, G.; Bachman, M.; Beraldi, D.; Balasubramanian, S. *Nat. Chem.* **2014**, *6*, 435−440.

https://doi.org/10.1021/acs.analchem.1c01285
Anal. Chem. 2021, 93, 10495−10501